

Symmetry Breaking and the Molecular Structure of $\text{NO}_3^{+\dagger}$

Charles E. Miller*

Department of Chemistry, Haverford College, Haverford, Pennsylvania 19041-1392

Joseph S. Francisco[‡]

Department of Chemistry and Department of Earth and Atmospheric Science, Purdue University, West Lafayette, Indiana 47907-1393

Received: June 30, 2000; In Final Form: November 29, 2000

The equilibrium structure and vibrational frequencies of the nitrate cation, NO_3^+ , have been investigated with an extensive set of ab initio calculations. Two stationary points were identified on the NO_3^+ potential energy surface: a symmetric D_{3h} structure and a C_{2v} ring structure similar to that found for the isoelectronic CO_3 molecule. Geometry optimizations executed at the CCSD(T)/aug-cc-pVTZ level of theory yielded the following data. $\text{NO}_3^+(D_{3h})$: $E_{\text{rel}} = 2130 \text{ cm}^{-1}$, $r_e = 1.238 \text{ \AA}$. $\text{NO}_3^+(C_{2v})$: $E_{\text{rel}} = 0 \text{ cm}^{-1}$, $r_1 = 1.131 \text{ \AA}$, $r_2 = r_3 = 1.309 \text{ \AA}$, $\theta = 142.3^\circ$. Calculations performed at the B3LYP, QCISD, CCSD, and CCSD(T) levels of theory all predict the C_{2v} structure to be lower in energy than the D_{3h} structure. Relative energy calculations performed with the Gaussian and complete basis set model chemistry algorithms also predict the C_{2v} structure to be the most stable NO_3^+ conformation. These results are supported by vibrational frequency calculations which suggest that the D_{3h} structure may correspond to a second-order saddle point rather than a true minimum on the NO_3^+ potential energy hypersurface. The symmetry breaking observed in the present NO_3^+ calculations is similar to that observed in ab initio studies of the NO_3 equilibrium structure and is used to examine symmetry breaking across the nitrate series NO_3^- , NO_3 , NO_3^+ .

Introduction

The importance of the nitrate radical (NO_3) in atmospheric chemistry has generated widespread interest in its chemical and physical properties.¹ In particular, the question of whether NO_3 possesses a D_{3h} or C_{2v} equilibrium structure has caused considerable controversy, with substantial experimental and theoretical support for each conclusion.^{2–28} Ab initio calculations have emphasized the difficulty of the symmetry breaking problem in NO_3 by demonstrating that the potential energy surface is extremely flat in the region of the D_{3h} minimum.^{22–27} Even the most sophisticated levels of theory could not conclusively establish the nature of the D_{3h} stationary point.²⁶

One might deduce the equilibrium structure of NO_3 by examining structural trends in the sequence NO_3^- , NO_3 , NO_3^+ . Addition of a valence electron to the NO_3 radical forms the well-known nitrate anion, NO_3^- . Overwhelming experimental evidence has established that NO_3^- possesses a D_{3h} structure with the equilibrium bond length ranging from 1.22 to 1.27 \AA , depending on the environment.²⁹ Unperturbed NO_3^- displays no instability with respect to distortion into a lower symmetry configuration. In contrast, Boehm and Lohr identified optimized NO_3^+ structures having both D_{3h} and C_{2v} symmetries in ab initio calculations performed at the Hartree–Fock (HF) level of theory with a double- ζ plus polarization (DZP) basis set.¹⁷ Boehm and Lohr also investigated the relative stabilities of the two structures by calculating single-point energies with Møller–Plesset perturbation theory at the optimized HF/DZP geometries. They found that the energy ordering of the two structures oscillated

with the order of perturbation employed, ultimately favoring the D_{3h} structure at the MP4SDTQ level of theory.¹⁷ Monks et al.¹⁵ argued that NO_3 and NO_3^+ possess virtually identical D_{3h} equilibrium structures on the basis of the sharp onset and lack of vibrational structure in the threshold region of their photoionization spectrum. Monks et al. also performed MCSCF calculations, based on the optimized structures calculated by Boehm and Lohr, from which they concluded that the theoretical evidence was unambiguous about the nitrate cation structure being D_{3h} .¹⁵ However, Heryadi and Yeager¹⁸ found reasonable agreement between experimental¹⁶ and theoretical ionization energies for NO_3^+ using either D_{3h} or C_{2v} structures, while Lee and Wright¹⁹ suggested that an ionic $[\text{NO}^+\cdots\text{O}_2]$ complex represents the most stable form of “ NO_3^+ ”. Thus, it appears that symmetry breaking complicates the structural characteristics of NO_3 and NO_3^+ and that the stable $\text{NO}_3^-(D_{3h})$ structure is the exceptional case.

There are several physical properties that make NO_3^+ more tractable to ab initio characterization than NO_3 . Many of the technical difficulties encountered in theoretical descriptions of the NO_3 radical arise due to the need to treat spatial and spin contributions to the electronic structure simultaneously. The ground state of NO_3^+ assumes a closed-shell electronic configuration. The resulting singlet state eliminates the spin contribution and assesses directly the impact that the electronic configuration has on the molecular geometry. This work presents a detailed ab initio investigation of NO_3^+ and its implications for the symmetry breaking problem in NO_3 .

Methods

All calculations were performed using the *Gaussian 98* program suite.³⁰ Ab initio structure optimizations and vibrational

[†] Part of the special issue “Harold Johnston Festschrift”.

* Corresponding author. Email: cmiller@haverford.edu.

[‡] Email: jfrancis@chem.purdue.edu.

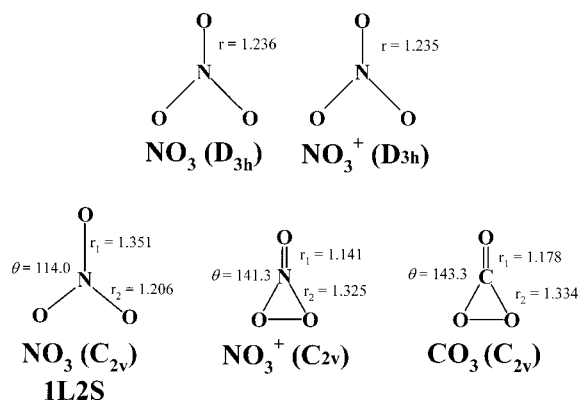


Figure 1. Structural comparison of the optimized $\text{NO}_3(D_{3h})$ (ref 25), $\text{NO}_3^+(D_{3h})$, $\text{NO}_3(C_{2v})$ (2L1S, ref 25), $\text{NO}_3^+(C_{2v})$, and CO_3 (ref 51) structures.

frequencies were calculated at the Hartree–Fock (HF), quadratic configuration interaction with single and double substitutions (QCISD),³¹ and coupled cluster (CCSD and CCSD(T))³¹ levels of theory. Further ab initio optimizations were performed with the Møller–Plesset perturbation theory (MPn), including the second-order Møller–Plesset with single and double excitations (MP2), the third-order Møller–Plesset with single and double excitations (MP3), the fourth-order Møller–Plesset with single, double, and quadruple excitations (MP4SDQ), and the fourth-order Møller–Plesset with single, double, triple, and quadruple excitations (MP4SDTQ).^{32–34} Additional structure optimizations and vibrational frequencies were calculated using the Becke3–Lee–Yang–Parr (B3LYP) density functional.³⁵ All geometry optimizations were converged to better than 0.001 Å for bond lengths and 0.1° for bond angles. Optimizations at the MP2, QCISD, and B3LYP levels of theory employed the analytical gradient method developed by Schlegel.³⁶ Optimizations performed using higher-order Møller–Plesset methods, CCSD, and CCSD(T) employed the eigenvalue following algorithm.^{37,38} The Pople 6-31G(d) to 6-311+G(3df)^{39–43} basis sets and Dunning’s correlation consistent basis sets^{44–48} were employed in this study. Harmonic vibrational frequencies were calculated analytically for the HF and B3LYP methods and numerically for all other levels of theory.

Results and Discussion

1. Geometry Optimizations. The NO_3^+ structure optimizations performed in this study were guided by previous theoretical work on NO_3 ^{17–28} and NO_3^+ .^{15–18} We initiated exploratory calculations at the Hartree–Fock level of theory from the optimized NO_3 geometries reported by Stanton et al.²⁵ Optimizations of the NO_3^+ equilibrium structure begun from the $\text{NO}_3(D_{3h})$ structure ($r_e = 1.236$ Å) yielded D_{3h} structures with r_e ranging from 1.17 to 1.18 Å. Optimizations of the NO_3^+ equilibrium structure begun from the NO_3 2L1S C_{2v} structure (two long and one short N–O bond lengths: $r_L = 1.266$ Å, $r_S = 1.198$ Å, $\theta_{\text{O}^*\text{NO}} = 126.4^\circ$) yielded C_{2v} ring structures similar to those found for the isoelectronic CO_3 molecule (Figure 1).^{49–51} Optimizations of the NO_3^+ equilibrium structure begun from the NO_3 1L2S C_{2v} structure (one long and two short N–O bond lengths: $r_L = 1.351$ Å, $r_S = 1.206$ Å, $\theta_{\text{O}^*\text{NO}} = 114.0^\circ$) resulted in dissociation and were not considered further. Note that none of these optimizations produced a $\text{NO}_3^+(C_{2v})$ structure similar to the one with 120° bond angles but different N–O bond lengths which Monks et al. identified.¹⁵ Geometry optimizations for other levels of theory were performed starting from the results of the HF or B3LYP calculations. The final

set of optimized $\text{NO}_3^+(D_{3h})$ and $\text{NO}_3^+(C_{2v})$ structures are summarized in Tables 1 and 2, respectively.

Basis set effects were evaluated by optimizing the NO_3^+ structures for each basis set with each theoretical method. The results in Tables 1 and 2 demonstrate that for each level of theory the optimized geometries systematically approach a single structure as the basis set size increased. This structural convergence was typically observed with the 6-311+G(2df) and aug-cc-pVTZ basis sets. Similar structures were also obtained with smaller basis set calculations, but these appear to occur accidentally rather than from complete structural convergence.

Closer examination of Tables 1 and 2 shows that the largest structural changes are associated with the addition of polarization functions. For example, the N–O bond lengths of the D_{3h} conformers generally contract by 0.010–0.015 Å upon expanding the basis set from 6-31G(d) to 6-311G(d). This structural change is accompanied by an energy stabilization of 0.1–0.3 hartrees. Augmenting the basis with additional *d*- or *f*-functions changes the bond lengths by a few thousandths of an Angstrom at most. Diffuse functions have little effect on the optimized D_{3h} geometries, despite the importance of lone-pair electrons in NO_3^+ . For the correlation-consistent basis sets, an increase from cc-pVDZ to cc-pVTZ causes a contraction of 0.005–0.010 Å in the N–O bond length and stabilizes the energy by as much as 0.25 hartrees, depending on the level of theory.

These trends contrast with the results of the C_{2v} calculations where there is larger sensitivity to the basis set changes. The N–O bond lengths r_1 and r_2 contract by 0.010–0.015 Å upon expanding the basis set from 6-31G(d) to 6-311G(d), similar to the behavior observed for the D_{3h} conformers. Adding a second *d*-function to the basis leaves r_1 relatively unchanged but causes r_2 to elongate by as much as 0.010 Å. Expanding the basis set from 6-311+G(2d) to 6-311+G(2df) causes r_2 to recontract by approximately 0.010 Å, offsetting the elongation observed in the previous basis set expansion. Augmenting the basis set with additional *d*-functions produces minimal changes in the optimized structures. Increasing the basis set size from cc-pVDZ to cc-pVTZ induces contraction in both r_1 and r_2 . Interestingly, the bond angle typically varies by no more than 0.5° over all basis set changes.

Comparing the fully optimized NO_3^+ structures shows that the geometries converge across levels of theory. The optimized $\text{NO}_3^+(D_{3h})$ structures obtained at the B3LYP, QCISD, and CCSD levels of theory agree quite well, all predicting equilibrium N–O bond lengths $r_e \approx 1.215$ Å. The r_e value calculated at the B3LYP/6-311+G(3df) and QCISD/6-311+G(3df) levels of theory only differ by 0.002 Å, while the r_e value calculated at the CCSD/6-311+G(3df) level of theory is less than 0.004 Å longer than the QCISD/6-311+G(3df) value. These results contrast sharply with the HF/6-311+G(3df) optimization, which yields the significantly shorter result $r_e = 1.171$ Å, consistent with previously reported HF results.^{15,17}

Structure optimizations for $\text{NO}_3^+(D_{3h})$ performed at the CCSD(T) level of theory illustrate the importance of triple excitations. The optimized CCSD(T) geometries yield N–O bond lengths that are generally 0.023 Å longer than the CCSD geometries calculated with the same basis sets. Stanton and co-workers found that large basis sets and triple excitations were indispensable to the correct description of $\text{NO}_3(D_{3h})$.^{25–27} The present results indicate that an accurate theoretical characterization of $\text{NO}_3^+(D_{3h})$ also requires large basis sets and a treatment of the electron correlation extending through triple excitations.

The importance of extended electron correlation is also manifest in the $\text{NO}_3^+(C_{2v})$ calculations. The optimized B3LYP,

TABLE 1: Optimized Structures and Energies for $\text{NO}_3^+(D_{3h})$

theory/basis set	R(NO)/Å	energy/hartrees	theory/basis set	R(NO)/Å	energy/hartrees
HF/6-31G(d)	1.179	-278.21396	MP4SDQ/6-311G(2d)	1.221	-279.20786
HF/6-311G(d)	1.174	-278.28928	MP4SDQ/6-31+G(d)	1.026	-278.71155
HF/6-311G(2d)	1.172	-278.30698	MP4SDQ/6-311+G(d)	1.224	-279.16161
HF/6-31+G(d)	1.180	-278.22007	MP4SDQ/6-311+G(2d)	1.222	-279.21575
HF/6-311+G(d)	1.174	-278.29441	MP4SDQ/6-311+G(2df)	1.215	-279.29108
HF/6-311+G(2d)	1.173	-278.31099	MP4SDQ/6-311+G(3df)	1.214	-279.30446
HF/6-311+G(2df)	1.172	-278.32238	MP4SDQ/cc-pVDZ	1.226	-279.06644
HF/6-311+G(3df)	1.171	-278.32634	MP4SDQ/cc-pVTZ	1.216	-279.30676
B3LYP/6-31G(d)	1.228	-279.72081	MP4SDQ/aug-cc-pVDZ	1.228	-279.11870
B3LYP/6-311G(d)	1.221	-279.79851	QCISD/6-31G(d)	1.234	-279.02374
B3LYP/6-311G(2d)	1.220	-279.81140	QCISD/6-311G(d)	1.222	-279.15277
B3LYP/6-31+G(d)	1.228	-279.72710	QCISD/6-311G(2d)	1.222	-279.20993
B3LYP/6-311+G(d)	1.222	-279.80336	QCISD/6-31+G(d)	1.235	-279.03557
B3LYP/6-311+G(2d)	1.221	-279.81531	QCISD/6-311+G(d)	1.224	-279.16175
B3LYP/6-311+G(2df)	1.219	-279.82312	QCISD/6-311+G(2d)	1.223	-279.21744
B3LYP/6-311+G(3df)	1.218	-279.82608	QCISD/6-311+G(2df)	1.217	-279.29425
B3LYP/cc-pVDZ	1.224	-279.75087	QCISD/6-311+G(3df)	1.216	-279.30791
B3LYP/cc-pVTZ	1.219	-279.83138	QCISD/cc-pVDZ	1.226	-279.06856
B3LYP/aug-cc-pVDZ	1.225	-279.77015	QCISD/cc-pVTZ	1.218	-279.30992
B3LYP/aug-cc-pVTZ	1.219	-279.83444	QCISD/aug-cc-pVDZ	1.229	-279.12134
MP2/6-31G(d)	1.294	-279.15102	QCISD/aug-cc-pVTZ	1.218	-279.30992
MP2/6-311G(d)	1.280	-279.34484	CCSD/6-31G(d)	1.230	-279.01651
MP2/6-311G(2d)	1.280	-279.41445	CCSD/6-311G(d)	1.218	-279.14481
MP2/6-31+G(d)	1.294	-279.16474	CCSD/6-311G(2d)	1.218	-279.20228
MP2/6-311+G(d)	1.280	-279.35570	CCSD/6-31+G(d)	1.230	-279.02817
MP2/6-311+G(2d)	1.281	-279.42282	CCSD/6-311+G(d)	1.219	-279.15369
MP2/6-311+G(2df)	1.272	-279.49917	CCSD/6-311+G(2d)	1.219	-279.20967
MP2/6-311+G(3df)	1.269	-279.51966	CCSD/6-311+G(2df)	1.213	-279.28677
MP2/cc-pVDZ	1.286	-279.18887	CCSD/6-311+G(3df)	1.212	-279.30043
MP2/cc-pVTZ	1.272	-279.48398	CCSD/cc-pVDZ	1.222	-279.06147
MP2/aug-cc-pVDZ	1.285	-279.24544	CCSD/cc-pVTZ	1.214	-279.30231
MP2/aug-cc-pVTZ	1.270	-279.51163	CCSD/aug-cc-pVDZ	1.225	-279.11432
MP3/6-31G(d)	1.209	-278.98237	CCSD/aug-cc-pVTZ	1.214	-279.31930
MP3/6-311G(d)	1.198	-279.10948	CCSD(T)/6-31G(d)	1.253	-279.08712
MP3/6-311G(2d)	1.198	-279.17058	CCSD(T)/6-311G(d)	1.241	-279.22230
MP3/6-31+G(d)	1.210	-278.99270	CCSD(T)/6-311G(2d)	1.242	-279.28480
MP3/6-311+G(d)	1.198	-279.11744	CCSD(T)/6-31+G(d)	1.254	-279.10017
MP3/6-311+G(2d)	1.199	-279.17725	CCSD(T)/6-311+G(d)	1.242	-279.23227
MP3/6-311+G(2df)	1.195	-279.25983	CCSD(T)/6-311+G(2d)	1.243	-279.29298
MP3/6-311+G(3df)	1.194	-279.27394	CCSD(T)/6-311+G(2df)	1.236	-279.37290
MP3/cc-pVDZ	1.202	-279.02929	CCSD(T)/6-311+G(3df)	1.235	-279.38766
MP3/cc-pVTZ	1.195	-279.27571	CCSD(T)/cc-pVDZ	1.244	-279.13100
MP3/aug-cc-pVDZ	1.206	-279.08333	CCSD(T)/cc-pVTZ	1.237	-279.38936
MP4SDQ/6-31G(d)	1.234	-279.02210	CCSD(T)/aug-cc-pVDZ	1.248	-279.18906
MP4SDQ/6-311G(d)	1.223	-279.15227	CCSD(T)/aug-cc-pVTZ	1.237	-279.40824

QCISD, and CCSD geometries converge toward a single C_{2v} ring structure with $r_1 \approx 1.131$ Å, $r_2 \approx 1.310$ Å, and $\theta \approx 142.3^\circ$. However, a comparison of the CCSD and CCSD(T) calculations shows that the CCSD(T) structures predict an elongation of r_1 by ~ 0.010 Å, an elongation of r_2 by ~ 0.015 Å, and a contraction of θ by $\sim 1.0^\circ$. The $\text{NO}_3^+(C_{2v})$ geometries calculated at the HF level of theory significantly underestimate the values obtained with more extensive treatments of the electron correlation, as was the case with $\text{NO}_3^+(D_{3h})$.

The identification of optimized $\text{NO}_3^+(D_{3h})$ and $\text{NO}_3^+(C_{2v})$ structures across all levels of theory indicates that the NO_3^+ potential energy surface supports multiple stationary points. Ab initio wave functions describing NO_3^+ are thus likely to exhibit symmetry breaking. Unlike the NO_3 radical, the D_{3h} and C_{2v} geometries of NO_3^+ possess dramatically different structural characteristics, implying that the symmetry breaking in this system could be considerable.

2. Energetics and Vibrational Frequencies. The question of whether the minimum-energy NO_3^+ structure possesses D_{3h} or C_{2v} symmetry was first addressed by Boehm and Lohr.¹⁷ They optimized both the $\text{NO}_3^+(D_{3h})$ and $\text{NO}_3^+(C_{2v})$ structures at the HF/DZP level of theory and then employed these structures in a series of MPn single-point energy calculations. On the basis

of the MP4SDTQ/DZP//HF/DZP energies, Boehm and Lohr concluded that $\text{NO}_3^+(D_{3h})$ was the more stable structure.¹⁷ However, as shown in Tables 1 and 2 and discussed in Section 1, it appears that extensive electron correlation methods are required to obtain accurate NO_3^+ structures. Since the NO_3^+ structures optimized at the HF level of theory differ significantly from the CCSD(T) calculations, the conclusions Boehm and Lohr drew from their MPn//HF/DZP single-point calculations are questionable.

To investigate the performance of the MPn method for NO_3^+ , we calculated MPn/6-31G(d)//HF/6-31G(d) energies and $\Delta E(D_{3h} - C_{2v})$ for NO_3^+ . Figure 2a shows that the prediction of which NO_3^+ structure is most stable depends on the degree of perturbation invoked, as reported by Boehm and Lohr.¹⁷ We also performed full MPn/6-31G(d) optimizations of the D_{3h} and C_{2v} structures to determine if $\Delta E(D_{3h} - C_{2v})$ oscillated due to unrelaxed geometries. Figure 2b demonstrates that even the fully relaxed MPn structures exhibit fluctuations in the $(D_{3h} - C_{2v})$ energy difference as the degree of perturbation treatment varies. Figure 3 shows that the $\Delta E(D_{3h} - C_{2v})$ is well behaved as a function of basis set size for the MP2, MP3, and MP4SDQ levels of theory. The results collected in Tables 1 and 2 also show that the best MPn $\text{NO}_3^+(D_{3h})$ and $\text{NO}_3^+(C_{2v})$ structures deviate

TABLE 2: Optimized Structures and Energies for $\text{NO}_3^+(C_{2v})$

theory/basis set	R1/Å	R2/Å	A1/deg	energy/hartrees	theory/basis set	R1/Å	R2/Å	A1/deg	energy/hartrees
HF/6-31G(d)	1.111	1.274	143.6	-278.32064	MP4SDQ/6-31+G(d)	1.152	1.327	141.6	-279.06943
HF/6-311G(d)	1.102	1.264	144.0	-278.39386	MP4SDQ/6-311+G(d)	1.139	1.311	141.5	-279.19347
HF/6-311G(2d)	1.101	1.264	143.7	-278.41384	MP4SDQ/6-311+G(2d)	1.137	1.321	141.6	-279.25314
HF/6-31+G(d)	1.111	1.274	143.7	-278.32697	MP4SDQ/6-311+G(2df)	1.133	1.310	142.0	-279.33436
HF/6-311+G(d)	1.102	1.265	144.0	-278.39968	MP4SDQ/6-311+G(3df)	1.133	1.307	142.1	-279.34783
HF/6-311+G(2d)	1.101	1.270	143.7	-278.41769	MP4SDQ/cc-pVDZ	1.143	1.317	141.3	-279.09919
HF/6-311+G(2df)	1.100	1.266	143.8	-278.43308	MP4SDQ/cc-pVTZ	1.134	1.311	142.1	-279.35159
HF/6-311+G(3df)	1.100	1.266	143.9	-278.43765	MP4SDQ/aug-cc-pVDZ	1.146	1.322	141.5	-279.15372
B3LYP/6-31G(d)	1.144	1.324	142.6	-279.74551	MP4SDQ/aug-cc-pVTZ				
B3LYP/6-311G(d)	1.134	1.316	142.5	-279.81869	QCISD/6-31G(d)	1.151	1.331	141.6	-279.05900
B3LYP/6-311G(2d)	1.133	1.320	142.6	-279.83517	QCISD/6-311G(d)	1.138	1.313	141.5	-279.18427
B3LYP/6-31+G(d)	1.144	1.324	142.6	-279.75085	QCISD/6-311G(2d)	1.136	1.323	141.7	-279.24579
B3LYP/6-311+G(d)	1.134	1.316	142.5	-279.82361	QCISD/6-31+G(d)	1.151	1.331	141.6	-279.07033
B3LYP/6-311+G(2d)	1.133	1.320	142.6	-279.83868	QCISD/6-311+G(d)	1.138	1.314	141.5	-279.19335
B3LYP/6-311+G(2df)	1.132	1.316	142.7	-279.84887	QCISD/6-311+G(2d)	1.136	1.323	141.6	-279.25273
B3LYP/6-311+G(3df)	1.131	1.315	142.8	-279.85210	QCISD/6-311+G(2df)	1.132	1.312	142.1	-279.33377
B3LYP/cc-pVDZ	1.139	1.319	142.6	-279.77256	QCISD/6-311+G(3df)	1.131	1.310	142.2	-279.34724
B3LYP/cc-pVTZ	1.132	1.317	142.7	-279.85827	QCISD/cc-pVDZ	1.142	1.321	141.3	-279.10023
B3LYP/aug-cc-pVDZ	1.140	1.321	142.7	-279.79330	QCISD/cc-pVTZ	1.133	1.313	142.2	-279.35081
B3LYP/aug-cc-pVTZ	1.131	1.318	142.8	-279.86140	QCISD/aug-cc-pVDZ	1.145	1.326	141.5	-279.15458
MP2/6-31G(d)	1.162	1.331	141.0	-279.08069	QCISD/aug-cc-pVTZ				
MP2/6-311G(d)	1.149	1.313	140.6	-279.27248	CCSD/6-31G(d)	1.149	1.326	141.8	-279.05252
MP2/6-311G(2d)	1.147	1.325	140.9	-279.34674	CCSD/6-311G(d)	1.135	1.308	141.8	-279.17757
MP2/6-31+G(d)	1.163	1.331	140.9	-279.09321	CCSD/6-311G(2d)	1.134	1.318	141.9	-279.23916
MP2/6-311+G(d)	1.149	1.314	140.6	-279.28209	CCSD/6-31+G(d)	1.149	1.325	141.8	-279.06372
MP2/6-311+G(2d)	1.147	1.325	140.9	-279.35423	CCSD/6-311+G(d)	1.136	1.309	141.8	-279.18654
MP2/6-311+G(2df)	1.142	1.314	141.2	-279.43629	CCSD/6-311+G(2d)	1.134	1.318	141.8	-279.24600
MP2/6-311+G(3df)	1.141	1.311	141.2	-279.45683	CCSD/6-311+G(2df)	1.130	1.307	142.2	-279.32758
MP2/cc-pVDZ	1.153	1.321	140.6	-279.11755	CCSD/6-311+G(3df)	1.130	1.305	142.3	-279.34105
MP2/cc-pVTZ	1.142	1.314	141.3	-279.42261	CCSD/cc-pVDZ	1.140	1.315	141.5	-279.09398
MP2/aug-cc-pVDZ	1.156	1.327	140.8	-279.17471	CCSD/cc-pVTZ	1.131	1.308	142.3	-279.34453
MP2/aug-cc-pVTZ	1.141	1.313	141.2	-279.44903	CCSD/aug-cc-pVDZ	1.143	1.320	141.7	-279.14833
MP3/6-31G(d)	1.143	1.314	142.4	-279.02993	CCSD/aug-cc-pVTZ	1.131	1.309	142.3	-279.36128
MP3/6-311G(d)	1.130	1.297	142.6	-279.15553	CCSD(T)/6-31G(d)	1.157	1.339	140.6	-279.09259
MP3/6-311G(2d)	1.128	1.306	142.5	-279.21851	CCSD(T)/6-311G(d)	1.145	1.322	140.1	-279.22364
MP3/6-31+G(d)	1.144	1.314	142.4	-279.04072	CCSD(T)/6-311G(2d)	1.143	1.333	140.6	-279.29070
MP3/6-311+G(d)	1.130	1.298	142.6	-279.16423	CCSD(T)/6-31+G(d)	1.158	1.339	140.5	-279.10485
MP3/6-311+G(2d)	1.128	1.307	142.5	-279.22516	CCSD(T)/6-311+G(d)	1.146	1.323	140.1	-279.23339
MP3/6-311+G(2df)	1.125	1.298	142.7	-279.31146	CCSD(T)/6-311+G(2d)	1.144	1.333	140.5	-279.29822
MP3/6-311+G(3df)	1.125	1.296	142.8	-279.32524	CCSD(T)/6-311+G(2df)	1.140	1.322	141.1	-279.38197
MP3/cc-pVDZ	1.135	1.304	142.3	-279.07276	CCSD(T)/6-311+G(3df)	1.139	1.320	141.2	-279.39629
MP3/cc-pVTZ	1.126	1.299	142.8	-279.32849	CCSD(T)/cc-pVDZ	1.149	1.330	140.0	-279.13381
MP3/aug-cc-pVDZ	1.137	1.309	142.4	-279.12793	CCSD(T)/cc-pVTZ	1.141	1.323	141.3	-279.39942
MP4SDQ/6-31G(d)	1.184	1.302	140.7	-279.05771	CCSD(T)/aug-cc-pVDZ	1.152	1.335	140.3	-279.19279
MP4SDQ/6-311G(d)	1.139	1.309	141.6	-279.18837	CCSD(T)/aug-cc-pVTZ	1.141	1.325	141.3	-279.41798
MP4SDQ/6-311G(2d)	1.137	1.320	141.6	-279.24623					

significantly from one another and from our best NO_3^+ structures, the CCSD(T)/aug-cc-pVTZ results. Since there is no obvious relationship between $\Delta E(D_{3h} - C_{2v})$ and the structural deviations as the degree of Møller–Plesset perturbation varies, we conclude that through the fourth order the MPn series fails to provide an accurate treatment of NO_3^+ . Furthermore, we cannot support the conclusion of Monks et al. that calculations at the MP4 level unambiguously show the symmetry of the minimum energy NO_3^+ structure to have D_{3h} symmetry.¹⁵

Figure 4 shows that the B3LYP, QCISD, CCSD, and CCSD(T) ($D_{3h} - C_{2v}$) energy differences exhibit reasonable behavior. The C_{2v} structure is predicted to be lower in energy than the D_{3h} structure for all four levels of theory. This contradicts the conclusion of Monks et al. regarding the MP4 calculations as well as their CAS-MCSCF calculations that placed $\text{NO}_3^+(D_{3h})$ 9090 cm^{-1} lower in energy than $\text{NO}_3^+(C_{2v})$.¹⁵ We note that Monks et al. did not verify the nature of the optimized NO_3^+ structures they obtained by calculating vibrational frequencies (see below). Calculations at the CCSD(T)/6-311+G(3df) level of theory place $\text{NO}_3^+(C_{2v})$ 1900 cm^{-1} below $\text{NO}_3^+(D_{3h})$; this difference increases to 2130 cm^{-1} at the CCSD(T)/aug-cc-pVTZ level of theory. The $\text{NO}_3^+(D_{3h} - C_{2v})$ energy difference was also evaluated using the Gaussian^{52–55} and complete basis

set^{56–61} model chemistries to verify the energetics obtained from the CCSD(T) calculations. The results in Table 3 show that the model chemistry calculations all indicate that the C_{2v} structure is lower in energy than the D_{3h} structure. The overwhelming weight of theoretical evidence thus predicts significant structural and energetic symmetry breaking in NO_3^+ .

Harmonic vibrational frequency calculations were performed to confirm that the optimized C_{2v} and D_{3h} structures represent true minima on the NO_3^+ potential energy surface. These results are presented in Tables 4 and 5. At the MP2 and MP3 levels of theory, we obtained reasonable values for the $\text{NO}_3^+(C_{2v})$ frequencies but unphysically large frequencies for one of the e' modes of $\text{NO}_3^+(D_{3h})$; the MP4SDQ and MP4SDTQ levels of theory yielded imaginary frequencies for this mode. The results from the MP2 and MP3 calculations are consistent with the MP2/6-31G(d) results reported by Lee and Wright¹⁹ and further emphasize the inadequacy of the MPn series for treating NO_3^+ .

The $\text{NO}_3^+(C_{2v})$ vibrational frequencies calculated at the B3LYP, QCISD, CCSD, and CCSD(T) levels of theory agree reasonably well, as shown in Table 4. Systematic exploration of the vibrational frequencies with the 6-31G(d) basis set demonstrates that $\text{NO}_3^+(C_{2v})$ is a true minimum energy structure for each of these levels of theory. Vibrational frequencies

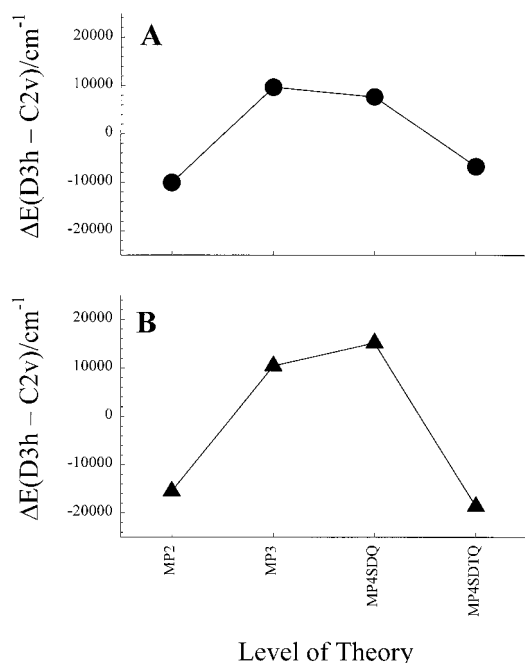


Figure 2. (A) NO_3^+ ($D_{3h} - C_{2v}$) energy differences determined for several MPn/6-31G(d)/HF/6-31G(d) calculations. (B) Same as in panel A, but energies now calculated using the NO_3^+ structures optimized at the specified MPn level of theory.

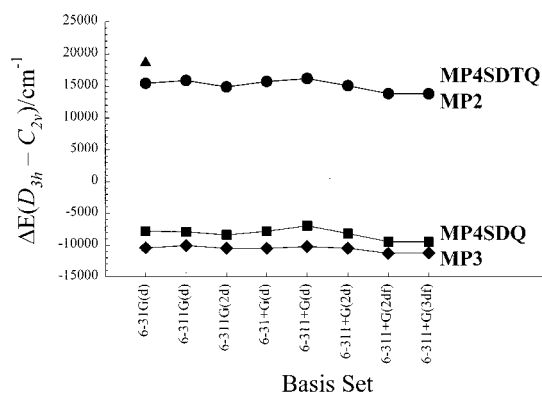


Figure 3. Convergence of the NO_3^+ ($D_{3h} - C_{2v}$) energy difference with increasing basis set size for calculations using the MP2, MP3, and MP4SDQ levels of theory. The MP4SDTQ/6-31G(d) energy point is included for reference to this level of theory.

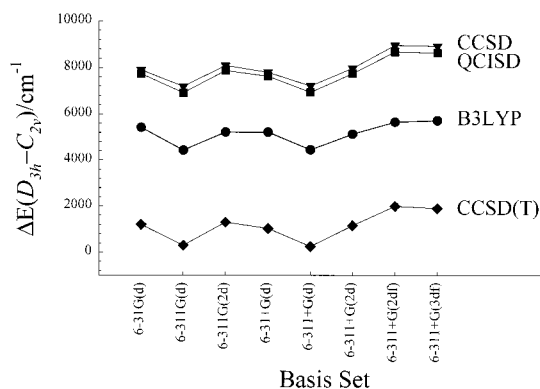


Figure 4. Convergence of the NO_3^+ ($D_{3h} - C_{2v}$) energy difference with increasing basis set size for calculations using the B3LYP, QCISD, CCSD, and CCSD(T) levels of theory.

calculated at the B3LYP/6-311+G(3df) and CCSD(T)/6-311+G(3df) levels are in good agreement with the 6-31G(d) calculations conducted using these two methods. Closer examination

TABLE 3: Model Chemistry Energies (0 K) for NO_3^+

method	NO_3^+ (C_{2v}) (hartrees)	NO_3^+ (D_{3h}) (hartrees)	$\Delta E(D_{3h} - C_{2v})$ (cm^{-1})
G1	-279.44389	-279.42974	3105
G2MP2	-279.43579	-279.42371	2651
G2	-279.44269	-279.42904	2995
G3B3	-279.63585	-279.63174	903
CBS-q	-279.50633	-279.50322	683
CBS-Q	-279.45797	-279.44525	2791
CBS-QB3	-279.45874	-279.44983	1954

TABLE 4: Vibrational Frequencies (cm^{-1}) Calculated for $\text{NO}_3^+(D_{3h})$

theory/basis set ^a	$\omega_1(a_1')$	$\omega_2(a_2'')$	$\omega_3(e')$	$\omega_4(e')$
MP2/6-31G(d)	891	615	567	10166
MP3/6-31G(d)	1306	773	668	7349
MP4SDQ/6-31G(d)	725	4260i	{1540, 488}	{1605i, 2535i}
MP4SDTQ/6-31G(d)	684	473	{713, 704}	{2588i, 2583i}
B3LYP/6-31G(d)	1149	729	1354	296
QCISD/6-31G(d)	2157	720	{820, 240}	{35460i, 28266i}
CCSD/6-31G(d)	1171	762	{854, 869}	{2588i, 2929i}

^a The CCSD(T)/6-31G(d) vibrational frequency calculation failed to converge.

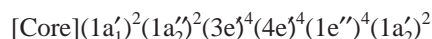
TABLE 5: Vibrational Frequencies (cm^{-1}) Calculated for $\text{NO}_3^+(C_{2v})$

theory/basis set	$\omega_1(a_1)$	$\omega_2(a_1)$	$\omega_3(a_1)$	$\omega_4(b_2)$	$\omega_5(b_2)$	$\omega_6(b_1)$
MP2/6-31G(d)	1803	1052	646	971	642	534
MP3/6-31G(d)	2046	1150	688	1026	561	612
MP4SDQ/6-31G(d)	2407	1251	687	988	489	1853i
MP4SDTQ/6-31G(d)	1784	968	549	795	501	627
B3LYP/6-31G(d)	2009	1105	690	902	531	612
QCISD/6-31G(d)	1986	1039	578	972	538	607
CCSD/6-31G(d)	2004	1076	610	1004	548	612
CCSD(T)/6-31G(d)	1908	990	487	937	521	601
B3LYP/6-311+G(3df)	2001	1101	697	888	540	628
CCSD(T)/6-311+G(3df)	1943	1032	541	952	544	625

of the values in Table 4 shows that the vibrational frequencies change by less than 5% when increasing the basis set from 6-31G(d) to 6-311+G(3df) and that there are no gross changes in the normal mode assignments. The CCSD(T)/6-311+G(3df) frequencies should be considered as the most accurate values obtained in the present work.

In contrast, agreement among the $\text{NO}_3^+(D_{3h})$ vibrational frequency calculations is poor, especially for the degenerate modes ω_3 and ω_4 . The QCISD/6-31G(d) and CCSD/6-31G(d) calculations produce large, imaginary frequencies for ω_4 , and the CCSD(T)/6-31G(d) calculations failed to converge. At the B3LYP/6-31G(d) level, all of the vibrational frequencies are positive, and the problematic ω_4 mode has a value of 296 cm^{-1} . The B3LYP calculation returns a real vibrational frequency for ω_4 because the density functional methodology tends to avoid artificial spatial symmetry breaking in the equilibrium geometry region even when the unrestricted HF wave function breaks symmetry, as discussed by Sherrill et al. for NO_3 .⁶² The B3LYP calculation would therefore be less susceptible to the symmetry-breaking effects that affect the QCISD, CCSD, and CCSD(T) methods. However, it is well-known that the B3LYP method encounters difficulties in correctly describing the properties of transition states and saddle points. Our QCISD and CCSD results, coupled with the failure of the CCSD(T) calculation to converge successfully, suggest that the D_{3h} structure represents a second-order saddle point on the NO_3^+ potential energy surface rather than a true minimum. Thus, the vibrational frequency calculations also favor the C_{2v} structure as the true minimum and may be interpreted as an additional manifestation of symmetry breaking in NO_3^+ .

3. Symmetry Breaking in NO₃ and NO₃⁺. The difficulties in characterizing the equilibrium structures for the nitrate series NO₃⁻, NO₃, NO₃⁺ poses an interesting chemical problem. The nitrate anion NO₃⁻ possesses the 24-electron molecular orbital configuration



that results in a robust *D*_{3h} equilibrium structure. The removal of a single electron from the 1a₂' orbital induces second-order Jahn–Teller interactions and creates nearly isoenergetic *D*_{3h} and *C*_{2v} minima in the NO₃ radical.^{23–27} This was elegantly demonstrated in the photoelectron spectra of NO₃⁻ recorded by Weaver et al.¹¹ The very flat nature of the NO₃ potential energy surface in the *D*_{3h} region leads to structural instability and manifests itself as the well-known NO₃ symmetry breaking problem.^{22–27} The ionization of NO₃ into NO₃⁺ results in the loss of the unpaired 1a₂' electron. One might anticipate that the NO₃⁺ electron configuration [Core](1a₁')²(1a₂'')²(3e')⁴(4e'')⁴(1e'')⁴ would favor further distortion away from the symmetric *D*_{3h} geometry into a stable *C*_{2v} structure, but the available photoionization data suggests that NO₃⁺ assumes a *D*_{3h} configuration.^{15,16}

The ab initio calculations performed in the present study clearly indicate that the *C*_{2v} ring structure corresponds to the minimum energy NO₃⁺ configuration. The 2130 cm⁻¹ Δ*E*(*D*_{3h} – *C*_{2v}) calculated at the CCSD(T)/aug-cc-pVTZ level of theory is 1 order of magnitude larger than the Δ*E*(*D*_{3h} – *C*_{2v}) in NO₃ and demonstrates the degree of symmetry breaking in NO₃⁺. The large structural differences between the optimized *D*_{3h} and *C*_{2v} structures further emphasize the symmetry breaking in NO₃⁺: the planar configuration about the nitrogen atom is maintained, but the *C*_{2v} structure resembles a nitrosyl ring compound analogous to the carbonyl ring structure calculated for the isoelectronic CO₃ complex^{49–51} (see Figure 1). We found no stable Y-shaped NO₃⁺ structure with angles deviating slightly from 120°, similar to the 1L2S or 2L1S structures reported by Stanton et al.²⁵ for NO₃.

The optimized NO₃⁺(*C*_{2v}) structure differs so markedly from the X(2A₂')NO₃(*D*_{3h}) structure that the Franck–Condon factors linking the two structures should be small. Thus, one might expect that the threshold region of the photoionization spectrum would be dominated by NO₃(*D*_{3h}) → NO₃⁺(*D*_{3h}) transitions but that the transitions would exhibit vibrational progressions. The behavior of the photoionization spectrum at higher energies may display characteristics representative of both NO₃⁺(*D*_{3h}) and NO₃⁺(*C*_{2v}) structures, as suggested by Heryadi and Yeager.¹⁸ It appears that the contradiction between the experimental photoionization spectrum and the theoretical results for NO₃⁺ cannot be resolved at present.

Conclusions

Ab initio calculations have revealed that there is a significant symmetry-breaking problem associated with the equilibrium structure of the NO₃⁺ cation. Sophisticated electron correlation and model chemistry methods predict that the lowest-energy NO₃⁺ structure possesses *C*_{2v} symmetry and is analogous to the ground-state structure of the isoelectronic CO₃ complex. The energy difference between the NO₃⁺(*C*_{2v}) and NO₃⁺(*D*_{3h}) structures varies with the degree of electron correlation employed but exceeds 2100 cm⁻¹ at the CCSD(T)/aug-cc-pVTZ level of theory; this is a factor of 10 larger than the 200 cm⁻¹ Δ*E*(*D*_{3h} – *C*_{2v}) calculated for NO₃.²⁷ Vibrational analysis demonstrates that the *C*_{2v} structure is a true minimum on the

NO₃⁺ potential energy surface while the *D*_{3h} structure corresponds to a second-order saddle point. The structural instability of NO₃⁺ with respect to distortion away from *D*_{3h} geometries is a real result, reproducible using QCISD, CCSD, and CCSD-(T) levels of theory and independent of the basis set. This suggests that symmetry breaking also occurs in the NO₃ radical but that the purely electronic contributions to its molecular structure may be masked by competing constraints imposed by the electron spin considerations.

Note Added in Proof

Since the completion of our NO₃⁺ work, Eisfeld and Morokuma reported a detailed study of the symmetry-breaking effect in the NO₃ radical.⁶³ They observed that the “tenacious symmetry breaking” of the NO₃ electronic wave function persists for all methods employing single configurations but can be avoided by a complete active space (CAS) or multireference configuration interaction (MRCI) calculation. While CAS or MRCI calculations are beyond the scope of the present work, we have demonstrated that single-configuration calculations of NO₃⁺ are plagued by the same robust symmetry-breaking effects observed for NO₃. This suggests that sophisticated CAS or MRCI calculations may be able to resolve the structural questions surrounding the NO₃⁺ cation.

Acknowledgments. The authors are indebted to Professor Harold S. Johnston for inspiring them to investigate the spectroscopy and physical properties of the nitrogen oxides. The authors also wish to thank the NASA Jet Propulsion Laboratory for ample computing resources to conduct this research. The NASA Office of Space Science and Applications sponsors the Jet Propulsion Laboratory Super-Computer Project.

References and Notes

- Wayne, R. P.; Barnes, I.; Biggs, P.; Burrows, J. P.; Canosa Mas, C. E.; Hjorth, J.; Le-Bras, G.; Moortgat, G. K.; Perner, D.; Poulet, G.; Restelli, G.; Sidebottom, H. *Atm. Environ. A* **1991**, *1*.
- Ishiwata, T.; Fujiwara, I.; Naruge, Y.; Obi, K.; Tanaka, I. *J. Phys. Chem.* **1983**, *87*, 1349.
- Ishiwata, T.; Tanaka, I.; Kawaguchi, K.; Hirota, E. *J. Chem. Phys.* **1985**, *82*, 2196.
- Ishiwata, T.; Tanaka, I.; Kawaguchi, K.; Hirota, E. *J. Mol. Spectrosc.* **1992**, *153*, 1.
- Kawaguchi, K.; Hirota, E.; Ishiwata, T.; Tanaka, I. *J. Chem. Phys.* **1990**, *93*, 951.
- Kawaguchi, K.; Ishiwata, T.; Tanaka, I.; Hirota, E. *Chem. Phys. Lett.* **1991**, *180*, 436.
- Kawaguchi, K.; Ishiwata, T.; Hirota, E.; Tanaka, I. *Chem. Phys.* **1998**, *231*, 2.
- Hirota, E.; Kawaguchi, K.; Ishiwata, T.; Tanaka, I. *J. Chem. Phys.* **1991**, *95*, 771.
- Hirota, E.; Ishiwata, T.; Kawaguchi, K.; Fujitake, M.; Ohashi, N.; Tanaka, I. *J. Chem. Phys.* **1997**, *107*, 2829.
- Fiedl, R. R.; Sander, S. P. *J. Phys. Chem.* **1987**, *91*, 2721.
- Weaver, A.; Arnold, D. W.; Bradforth, S. E.; Neumark, D. M. *J. Chem. Phys.* **1991**, *94*, 1740.
- Kim, B.; Hunter, P. L.; Johnston, H. S. *J. Chem. Phys.* **1992**, *96*, 4057.
- Carter, R. T.; Schmidt, K. F.; Bitto, H.; Huber, J. R. *Chem. Phys. Lett.* **1996**, *257*, 3.
- Valachovic, L.; Riehn, C.; Mikhaylichenko, K.; Wittig, C. *Chem. Phys. Lett.* **1996**, *258*, 5.
- Monks, P. S.; Stief, L. J.; Krauss, M.; Kuo, S. D.; Zhang, Z.; Klemm, R. B. *J. Phys. Chem.* **1994**, *98*, 10017.
- Wang, D.; Jiang, P.; Qian, X.; Hong, G. *J. Chem. Phys.* **1997**, *106*, 3003.
- Boehm, R. C.; Lohr, L. L. *J. Comput. Chem.* **1991**, *12*, 119.
- Heryadi, D.; Yeager, D. L. *J. Chem. Phys.* **2000**, *112*, 4572.
- Lee, E. P. F.; Wright, T. G. *Chem. Phys. Lett.* **2000**, *318*, 1.
- Kim, B.; Johnston, H. S.; Clabo, D. A., Jr.; Schaefer, H. F., III. *J. Chem. Phys.* **1988**, *88*, 3204.

- (21) Kim, B.; Hammond, B. L.; Lester, W. A., Jr.; Johnston, H. S. *Chem. Phys. Lett.* **1990**, *168*, 131.
- (22) Davy, R. D.; Schaefer, H. F., III. *J. Chem. Phys.* **1989**, *91*, 4410.
- (23) Kaldor, U. *Chem. Phys. Lett.* **1990**, *166*, 5.
- (24) Kaldor, U. *Chem. Phys. Lett.* **1991**, *185*, 1.
- (25) Stanton, J. F.; Gauss, J.; Bartlett, R. J. *J. Chem. Phys.* **1991**, *94*, 4084.
- (26) Stanton, J. F.; Gauss, J.; Bartlett, R. J. *J. Chem. Phys.* **1992**, *97*, 5554.
- (27) Crawford, T. D.; Stanton, J. F. *J. Chem. Phys.* **2000**, *112*, 7873.
- (28) Mayer, M.; Cederbaum, L. S.; Koppel, H. *J. Chem. Phys.* **1994**, *100*, 899.
- (29) Hehre, W. J.; Radom, L.; Schleyer, P. v. R.; Pople, J. A. *Ab Initio Molecular Orbital Theory*; John Wiley and Sons: New York, 1986.
- (30) Frisch, M. J.; Trucks, G. W.; Schlegel, H. B.; Scuseria, G. E.; Robb, M. A.; Cheeseman, J. R.; Zakrzewski, V. G.; Montgomery, J. A.; Stratmann, R. E.; Burant, J. C.; Dapprich, S.; Millam, J. M.; Daniels, A. D.; Kudin, K. N.; Strain, M. C.; Farkas, O.; Tomasi, J.; Barone, V.; Cossi, M.; Cammi, R.; Mennucci, B.; Pomelli, C.; Adamo, C.; Clifford, S.; Ochterski, J.; Petersson, G. A.; Ayala, P. Y.; Cui, Q.; Morokuma, K.; Malick, D. K.; Rabuck, A. D.; Raghavachari, K.; Foresman, J. B.; Cioslowski, J.; Ortiz, J. V.; Stefanov, B. B.; Liu, G.; Liashenko, A.; Piskorz, P.; Komaromi, I.; Gomperts, R.; Martin, R. L.; Fox, D. J.; Keith, T.; Al-Laham, M. A.; Peng, C. Y.; Nanayakkara, A.; Gonzalez, C.; Challacombe, M.; Gill, P. M. W.; Johnson, B. G.; Chen, W.; Wong, M. W.; Andres, J. L.; Head-Gordon, M.; Replogle, E. S.; Pople, J. A. *Gaussian 98*, A.3 ed.; Gaussian, Inc: Pittsburgh, PA, 1998.
- (31) Pople, J. A.; Head Gordon, M.; Raghavachari, K. *J. Chem. Phys.* **1987**, *87*, 5968.
- (32) Möller, C.; Plesset, M. S. *Phys. Rev.* **1934**, *46*, 4852.
- (33) Pople, J. A.; Seeger, R.; Krishnan, R. *Int. J. Quantum Chem. Symp.* **1977**, *11*, 149.
- (34) Krishnan, R.; Pople, J. A. *Int. J. Quantum Chem.* **1978**, *14*, 91.
- (35) Becke, A. D. *J. Chem. Phys.* **1993**, *98*, 5648.
- (36) Schlegel, H. B. *J. Chem. Phys.* **1986**, *84*, 4530.
- (37) Baker, J. *J. Comput. Chem.* **1986**, *7*, 385.
- (38) Baker, J. *J. Comput. Chem.* **1987**, *8*, 563.
- (39) Ditchfield, R.; Hehre, W. J.; Pople, J. A. *J. Chem. Phys.* **1971**, *54*, 724.
- (40) Hehre, W. J.; Ditchfield, R.; Pople, J. A. *J. Chem. Phys.* **1972**, *56*, 2257.
- (41) Hariharan, P. C.; Pople, J. A. *Mol. Phys.* **1974**, *27*, 209.
- (42) Gordon, M. S. *Chem. Phys. Lett.* **1980**, *76*, 163.
- (43) Hariharan, P. C.; Pople, J. A. *Theor. Chim. Acta* **1973**, *28*, 213.
- (44) Woon, D. E.; Dunning, T. H., Jr. *J. Chem. Phys.* **1993**, *98*, 1358.
- (45) Kendall, R. A.; Dunning, T. H., Jr.; Harrison, R. J. *J. Chem. Phys.* **1992**, *96*, 6796.
- (46) Dunning, T. H., Jr. *J. Chem. Phys.* **1989**, *90*, 1007.
- (47) Francisco, K. A.; Woon, D. E.; Dunning, T. H., Jr. *J. Chem. Phys.* **1994**, *100*, 7410.
- (48) Wilson, A. K.; van Mourik, T.; Dunning, T. H., Jr. *THEOCHEM* **1996**, *388*, 339.
- (49) Francisco, J. S.; Williams, I. H. *Chem. Phys.* **1985**, *95*, 373.
- (50) van de Guchte, W. J.; Zwart, J. P.; Mulder, J. J. C. *THEOCHEM* **1987**, *37*, 3.
- (51) Froese, R. D. J.; Goddard, J. D. *J. Phys. Chem.* **1993**, *97*, 7484.
- (52) Pople, J. A.; Head Gordon, M.; Fox, D. J.; Raghavachari, K.; Curtiss, L. A. *J. Chem. Phys.* **1989**, *90*, 5622.
- (53) Curtiss, L. A.; Jones, C.; Trucks, G. W.; Raghavachari, K.; Pople, J. A. *J. Chem. Phys.* **1990**, *93*, 2537.
- (54) Curtiss, L. A.; Raghavachari, K.; Trucks, G. W.; Pople, J. A. *J. Chem. Phys.* **1991**, *94*, 7221.
- (55) Curtiss, L. A.; Raghavachari, K.; Pople, J. A. *J. Chem. Phys.* **1993**, *98*, 1293.
- (56) Nyden, M. R.; Petersson, G. A. *J. Chem. Phys.* **1981**, *75*, 1843.
- (57) Petersson, G. A.; Al Laham, M. A. *J. Chem. Phys.* **1991**, *94*, 6081.
- (58) Petersson, G. A.; Tensfeldt, T. G.; Montgomery, J. A., Jr. *J. Chem. Phys.* **1991**, *94*, 6091.
- (59) Montgomery, J. A., Jr.; Ochterski, J. W.; Petersson, G. A. *J. Chem. Phys.* **1994**, *101*, 5900.
- (60) Ochterski, J. W.; Petersson, G. A.; Montgomery, J. A., Jr. *J. Chem. Phys.* **1996**, *104*, 2598.
- (61) Montgomery, J. A., Jr.; Frisch, M. J.; Ochterski, J. W.; Petersson, G. A. *J. Chem. Phys.* **1999**, *110*, 2822.
- (62) Sherrill, C. D.; Lee, M. S.; Head-Gordon, M. *Chem. Phys. Lett.* **2000**, *302*, 425.
- (63) Einfeld, W.; Morokuma, K. *J. Chem. Phys.* **2000**, *113*, 5587.